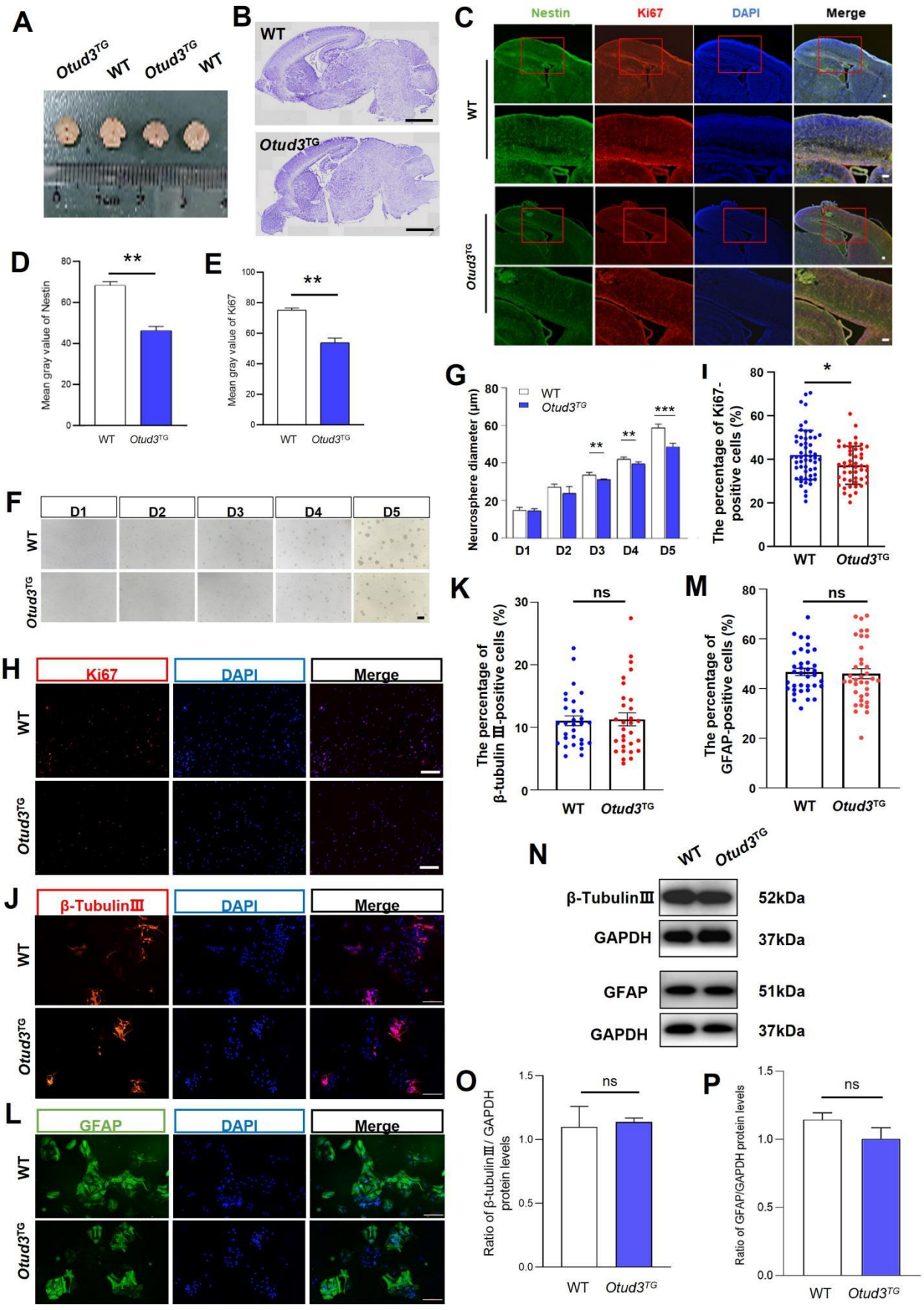

Figure S1. OTUD3 overexpression impairs NS/PCs proliferation and self-renewal during mouse cerebral

cortical development.

A: Gross morphology of E14-15 WT and *Otud3*^{TG} embryonic brains.

B: Nissl staining of sagittal sections from WT and *Otud3*^{TG} embryonic brains. Scale bar: 1 mm.

C: Immunofluorescence staining for Nestin and Ki67 in WT and *Otud3*^{TG} sagittal sections. Scale bar: 100 μm.

D, E: Quantification of mean gray values of Nestin (D) and Ki67 (E) immunofluorescence intensity (***P*<0.01, n=3, Student's t-test).

F: Representative images of neurospheres formed by WT and *Otud3*^{TG} NS/PCs at days 1–5 (D1–D5). Scale bars=100 μm.

G: Quantification of neurosphere diameter at D1–D5 (***P*<0.01 *****P*<0.0001, n=6, Student's t-test).

H: Immunofluorescence staining for Ki67 in WT and *Otud3*^{TG} neurospheres. Scale bar: 100 μm.

I: Quantification of the percentage of Ki67-positive cells in neurospheres (**P* < 0.05, n=55, Student's t-test).

J: Immunofluorescence staining for β-tubulin III in differentiated NS/PCs. Scale bar: 100 μm.

K: Quantification of the percentage of β-tubulin III-positive cells (ns, not significant, n=3,Student's t-test).

L: Immunofluorescence staining for GFAP in differentiated NSCs. Scale bar: 100 μm.

M: Quantification of the percentage of GFAP-positive cells (ns, not significant, n=3, Student's t-test).

N: Western blot analysis of β-tubulin III and GFAP protein levels in WT and *Otud3*^{TG} cortical samples.

O: Quantification of β-tubulin III/GAPDH and GFAP/GAPDH protein ratios (ns, not significant, n=3, Student's t-test).

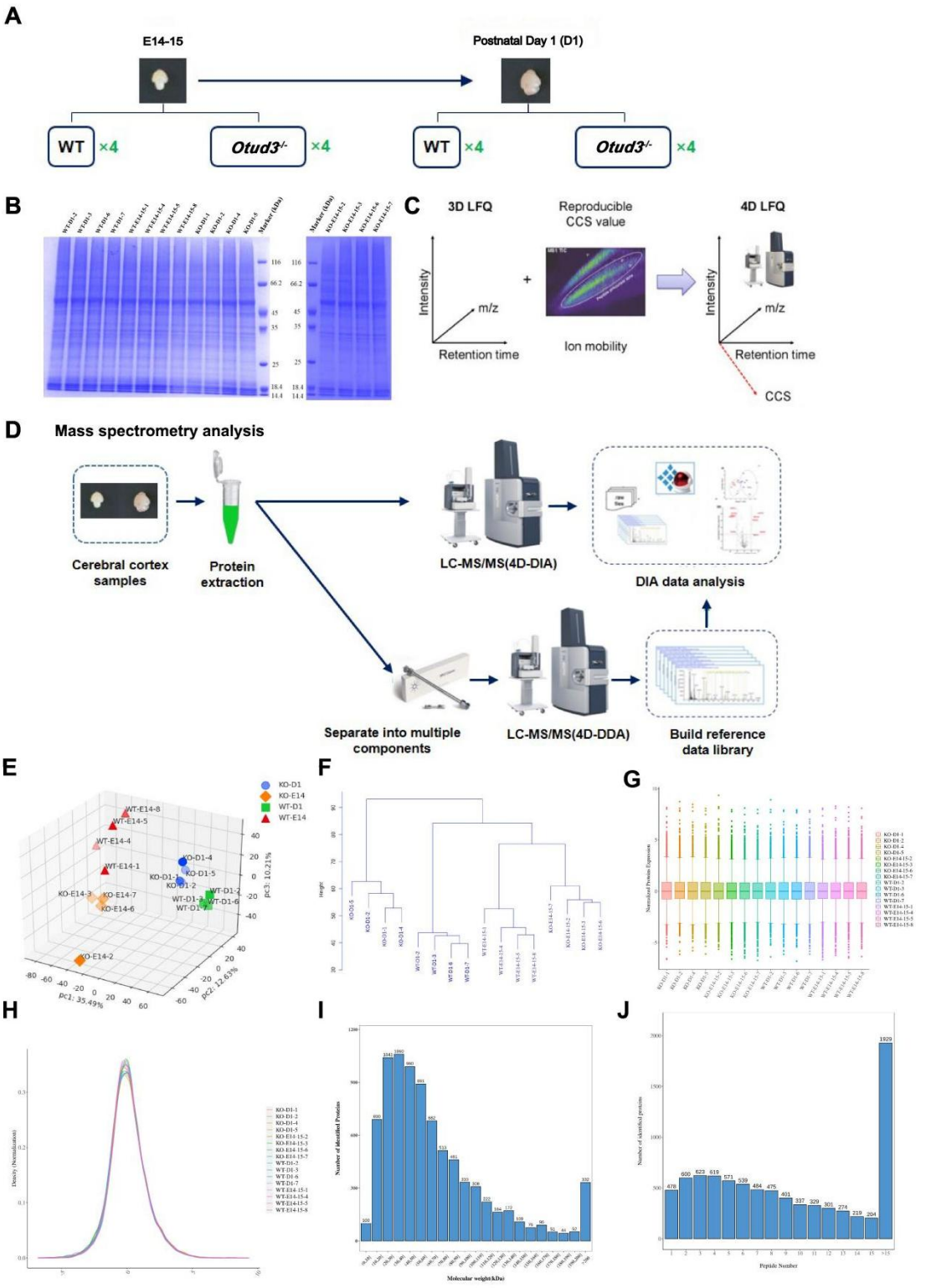

Figure S2. Experimental design and quality control of 4D proteomic analysis of WT and *Otud3*$^{-/-}$ mouse cerebral cortex.

A: Schematic of sample collection: cerebral cortex tissues were isolated from WT and *Otud3*$^{-/-}$ mice at E14-15 (n=4 per genotype) and D1 (n=4 per genotype).

B: SDS-PAGE analysis of total protein extracts from all samples, demonstrating consistent protein quality and loading. Molecular weight markers (kDa) are indicated.

C: Schematic comparison of 3D LFQ and 4D LFQ proteomic workflows. The 4D LFQ approach integrates ion mobility and CCS measurements to improve reproducibility and peptide identification.

D: Overview of the 4D proteomic pipeline: protein extraction from cerebral cortex samples, followed by 4D-DIA LC-MS/MS for quantitative analysis and 4D-DDA LC-MS/MS for reference library construction.

E: 3D PCA plot of proteomic data, showing separation of WT and *Otud3*$^{-/-}$ samples at E14-15 and D1.

F: Hierarchical clustering dendrogram of all samples, based on proteomic expression profiles.

G: Heatmap of sample-to-sample distance matrix, colored by genotype and developmental stage, confirming high within-group reproducibility.

H: Density plot of protein expression values, showing a normal distribution across the dataset.

I: Histogram of molecular weight distribution of identified proteins.

J: Histogram of unique peptide counts per identified protein.

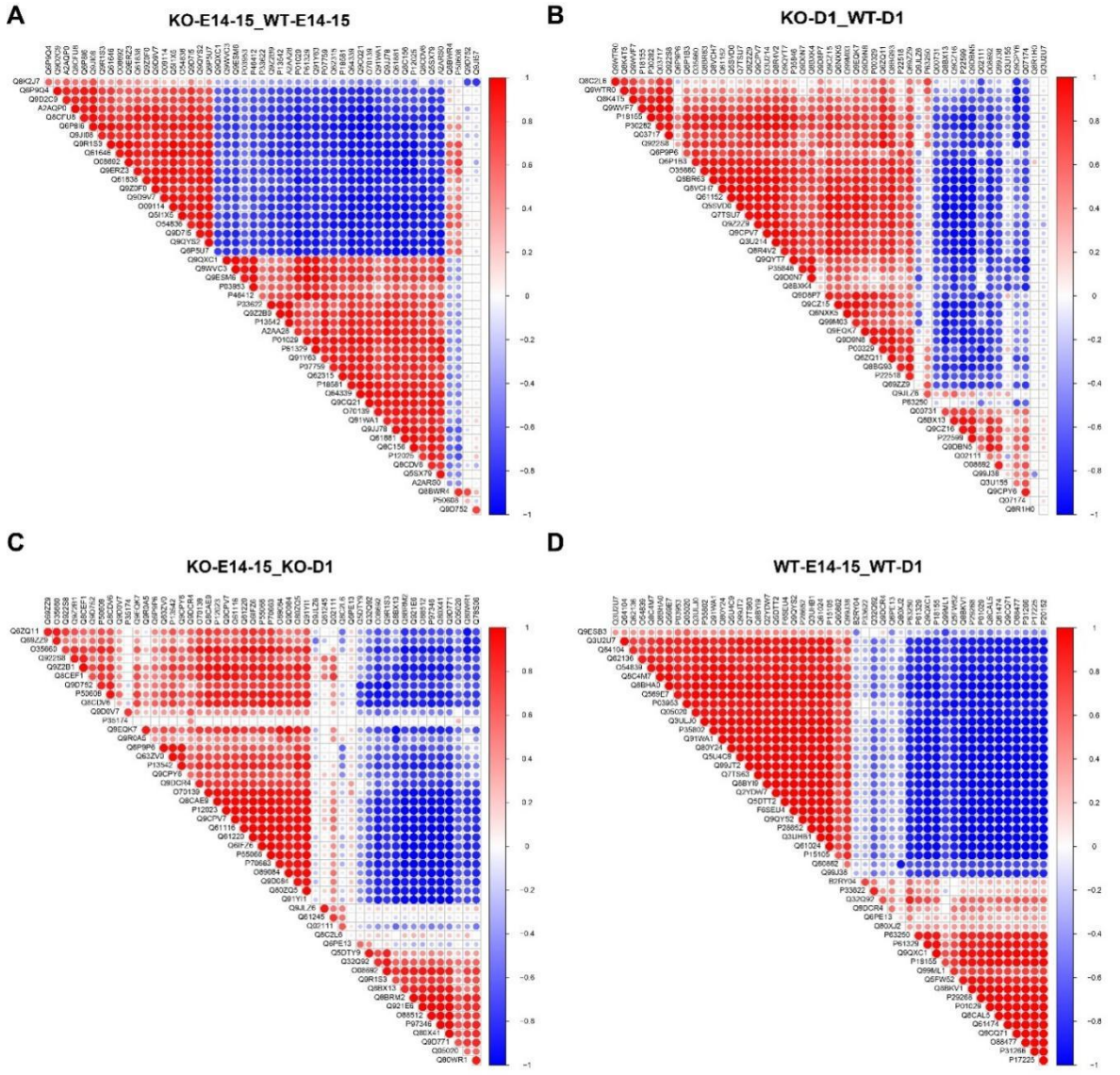

Figure S3. Pairwise correlation analysis of proteomic profiles across genotypes and developmental stages.

A: Correlation matrix comparing WT-E14-15 and KO-E14-15 samples. Color scale ranges from -1 (blue, perfect negative correlation) to 1 (red, perfect positive correlation).

B: Correlation matrix comparing WT-D1 and KO-D1 samples.

C: Correlation matrix comparing KO-E14-15 and KO-D1 samples, illustrating proteomic changes during postnatal development in *Otud3*$^{-/-}$ mice.

D: Correlation matrix comparing WT-E14-15 and WT-D1 samples, illustrating normal developmental proteomic changes in WT mice. All matrices are based on Pearson correlation coefficients of protein expression levels, with sample labels indicating genotype and developmental stage.

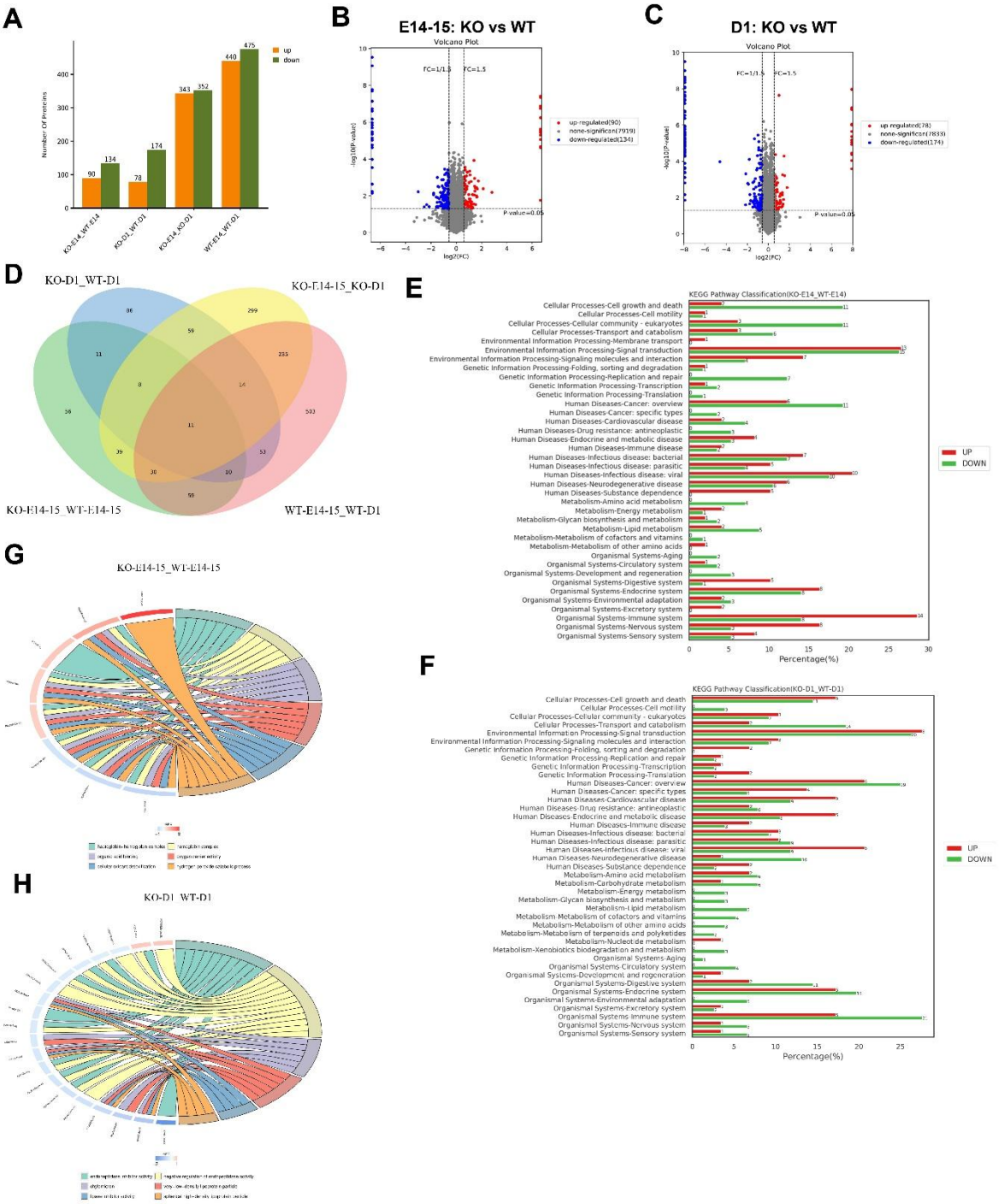

Figure S4. Differential proteomic analysis of developmental changes in WT and *Otud3*$^{-/-}$ mouse cerebral cortex.

A: Bar chart summarizing the number of DEPs in pairwise comparisons between WT and *Otud3*$^{-/-}$ mice cortex at E14-15 and D1. Upregulated (orange) and downregulated (green) proteins are displayed. **B,C:** Volcano plots illustrating genome-wide protein expression changes in *Otud3*$^{-/-}$ vs WT cortex at E14-15 (B) and D1 (C). Significantly up- (red) and downregulated (blue) DEPs are highlighted, with non-significant proteins shown in gray. **D:** Venn diagram showing overlap of DEPs across four

comparisons: KO-D1_WT-D1, KO-E14-15_KO-D1, WT-E14-15_WT-D1, and KO-E14-15_WT-E14-15. **E,F:** KEGG pathway classification of DEPs in KO vs WT cortex at E14-15 (E) and D1 (F). Proteins are categorized into functional pathway classes (e.g., cellular processes, human diseases, metabolism), with red and green bars representing the percentage of upregulated and downregulated proteins in each class, respectively.

G,H: Chord plots illustrating the functional connectivity between selected top 6 GO terms and their corresponding DEPs in (G) KO-E14-15_WT-E14-15 and (H) KO-D1_WT-D1 comparisons. Outer arc segments represent distinct GO terms (colored by functional category), and inner chords link each GO term to its associated DEPs (colored by functional category). The width of each chord is proportional to the number of DEPs annotated to the respective GO term.